Pergamon

PII: S0191-8141(98)00002-9

Journal of Structural Geology, Vol. 20, No. 5, pp. 491 to 502, 1998

0191-8141/98 $19.00 + 0.00

A rheological model for fractured rock

THOMAS L. PATTON

Amoco, P.O. Box 3092, Houston, TX 77253-3092, U.S.A.

and

RAYMOND C. FLETCHER

Department of Earth and Environmental Sciences, New Mexico Institute of Mining and Technology, Socorro, NM 87801, U.S.A.

(*Received* 27 *March* 1996; *accepted in revised form* 17 *December* 1997)

Abstract—We propose a rheological model for rock deforming in plane strain by slip on two sets of intersecting, weak surfaces. We assume that the normals to the surfaces lie within the deformation plane, and that the surfaces are unbounded and experience noninterfering slip. Where slip rate is linearly proportional to resolved shear stress, the rock behaves as an incompressible, anisotropic fluid. For the simplest case—where the intrinsic slip behavior along the two sets is identical—the principal axes of anisotropy are parallel and perpendicular to the bisectors of the intersurface angles. For deformation rates parallel and perpendicular to these axes, three behaviors may occur depending on the magnitude of the intersurface angle (2ϕ). If $0^\circ \leqslant 2\phi < 45^\circ$ or $135^\circ < 2\phi \leqslant 180^\circ$ the rock is weaker in shear than in shortening or extension. If $45^\circ < 2\phi < 135^\circ$ it is stronger in shear than in shortening or extension. Finally, if $2\phi = 45^\circ$ or 135°, the rock behaves isotropically. As applications, we use the derived constitutive relations to examine the response of a fractured layer to two commonly modeled types of folding: forced folding above a vertical fault and buckling of a layer embedded in an isotropic medium undergoing shortening.

INTRODUCTION

In mathematical models of structures, it is convenient to assume that the rocks behave as continua. However, in reality, they contain weak slip surfaces which may be active during deformation. The persistent recurrence of slip on major faults is perhaps the most often cited example of such behavior. For instance, some early Tertiary (Laramide) monoclines of the Colorado Plateau formed by slip on pre-existing faults of Precambrian age (Walcott, 1890; Reches, 1978). Another often cited example is the pervasive slip along pre-existing arrays of closely spaced, weak fracture surfaces. For instance, the early formed mineral-filled fractures found in granites of the west central Sierra Nevada Batholith, have accommodated left-lateral slip in a later tectonic episode (Segall and Pollard, 1983a). In the first example, deformation involves the reactivation of widely spaced major faults; in the second example, a pervasive fabric element is reactivated.

In this paper we propose a continuum description of a rock deforming primarily by the latter mechanism; specifically, slip on pervasive sets of pre-existing surfaces. We formulate a plane strain rheological model which predicts the response for two sets of intersecting surfaces, whose spacing is small relative to the scale of motions responsible for their deformation. We use the model to examine the effects of variations in the intersurface angle on the bulk rheological behavior of the rock mass. To illustrate the behavior, we model two examples of folding deformation of a fractured layer. The first examines forced folding of a fractured layer above a buried vertical fault; the second examines buckling instabilities of a fractured layer embedded in an isotropic medium.

CONSTITUTIVE RELATIONS FOR FRACTURED ROCK

Formulating a model for the rheological behavior of fractured rock is a formidable task. However, a useful model may be obtained with some simplifying approximations. Consider first the single set of roughly parallel fractures (Fig. 1) in granodiorite, documented in Segall and Pollard (1983b). The joints are open and mineral filled. The segment of their map shown in Fig. 1, is of an approximately horizontal surface showing fractures that are bounded in extent. Exposures of fractures on vertical cliffs have much the same appearance, and the fractures are probably equant in form, or 'penny-shaped'. In an area some 10 km from the example shown, filled joints of the same kind have been involved, as weak surfaces, in a subsequent deformation of the granodiorite (Segall and Pollard, 1983a). Many, but not all of the fractures in this area, show left-lateral displacements of a few centimeters to tens of centimeters, which involve shearing of the weak fracture-filling material. Since the fracture surfaces are bounded, slip implies an accommodating deformation of the otherwise coherent rock which contains them. If

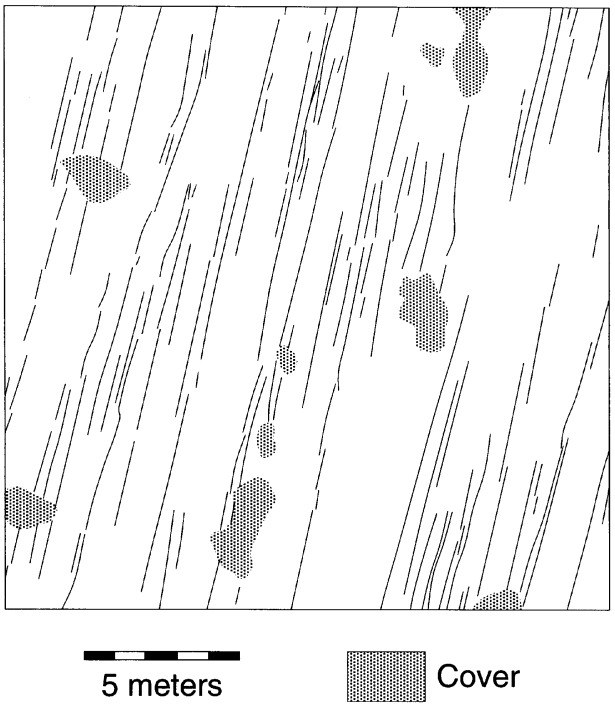

Fig. 1. Fracture geometry mapped from a horizontal surface in the Mount Givens Granodiorite of the Sierra Nevada Batholith. The map is a subset of fractures documented from maps of the Ward Lake outcrop compiled by Segall and Pollard (1983b). The fractures strike N10–20°E and dip steeply (70–90°) to the east.

the bulk shear of the rock is small, such accommodation may be purely elastic, but larger shear strain would require either local fracturing, linking of nearby fractures, or large local ductile strain. In the cited example, the first process dominates.

For comparison, an idealized fracture set is shown in Fig. 2(a). The fractures are parallel and unbounded. Thus, no accommodation mechanism is needed for slip (Fig. 2b) along the fractures. The macroscopic behavior, at a scale much larger than the joint spacing, depends only on the intrinsic joint surface behavior in slip. Here, we shall initially adopt this idealization. Evidently, slip accommodation must also lead to a continuous change in the relations between bulk strain rate and stress. This difficulty is also bypassed by considering the idealized configuration.

The intrinsic behavior of a fracture surface, or filled fracture, in shear might be approximated in several ways. Perhaps the most familiar model involves frictional behavior. The on–off character of frictional behavior—depending on whether the resolved shear stress is below or at the critical yield value—is not especially tractable from a mathematical point of view. However, the shearing of a weak fracture fill at moderately high temperatures, as in the example cited, can be treated in terms of a creep law. Alternatively, if slip is governed by dissolution and reprecipitation of a soluble phase around roughness elements, as suggested by fiber growth in the manner of diffusion-accommodated grain-boundary sliding, a linear viscous creep law might be appropriate. Since the latter is the simplest law, we shall use it. While the structure of fracture surfaces may favor slip in a particular direction—especially after some slip has already occurred—we shall assume no such directional dependence here.

The shear rate arising from slip on a single set of parallel surfaces (Fig. 2b), pervasive and uniformly developed at the scale of interest, is taken to be linearly proportional to the resolved shear stress. If rates of shearing on several such sets are tensorially summed, and if the number of independent sets is sufficient to admit an arbitrary deformation of the material, the constitutive relations for the material are those of an anisotropic linear viscous fluid. The components of the rate-of-deformation tensor, $\mathbf{D}_{ij}$, will be related to the components of the deviatoric stress

$$\mathbf{s}_{ij} = \sigma_{ij} - (1/3)\sigma_{kk}\delta_{ij} \tag{1a}$$

by the linear relationship

$$\mathbf{D}_{ij} = \Lambda_{ijkl}\mathbf{s}_{kl} \tag{1b}$$

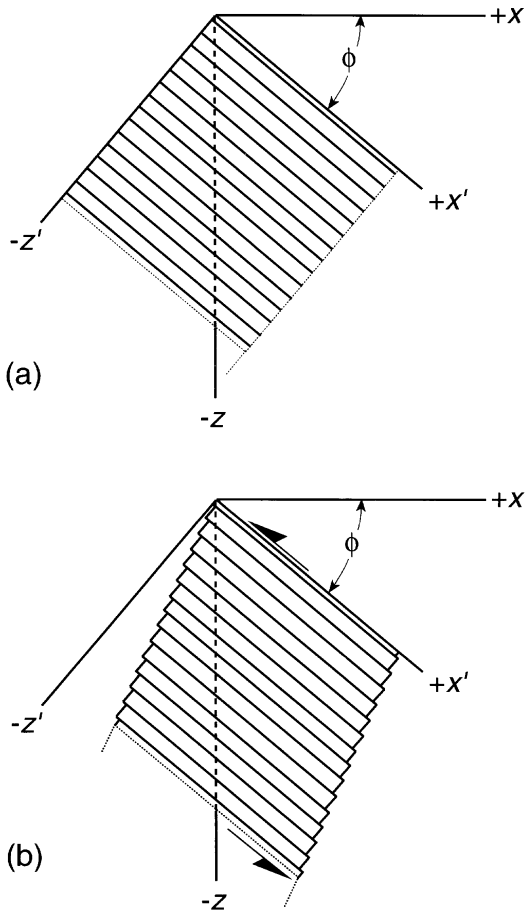

Fig. 2. Idealized, undeformed fracture array (a) composed of perfectly parallel, unbounded fractures as seen in a vertical outcrop. The fractures posses a dip ϕ, which, when measured in the fourth quadrant, is negative. The axes x' and z' are parallel and perpendicular to the fractures, respectively. The y- and y'-axes are identically equal and parallel to the strike of the fractures. Bulk deformation of the rock mass (b) by a uniform rate of slip along the fracture surfaces in the x' direction.

where the tensor Λ_{ijkl} might be termed the reciprocal viscosity tensor.

Note that here, we treat each set of weak surfaces as a 'slip system' in the sense used in crystal plasticity. This is clearly an approximation, and likely a crude one, since slip on one set of weak surfaces will disrupt the continuity of the others. Slip on multiple sets leads to the development of additional, accommodating structures (Robin and Currie, 1971) and most likely to strain-hardening behavior. For this reason, our model and existing models (Morland, 1976; Reches, 1979; Amadei and Goodman, 1981; Patton and Fletcher, 1983) have the major feature in common that they treat the slip on sets of fractures as independent and tensorially summable, ignoring interference which leads to hardening.

To illustrate our simple model, we consider a two-dimensional limiting case. Only two sets of surfaces are present, and the deformation is restricted to plane deformation in the plane normal to their line of intersection. (Another two-dimensional case, not treated here, would consist of antiplane deformation, with velocity parallel to the line of intersection.) Since the material is incompressible, there are only two independent components of the rate-of-deformation tensor, and two independent sets of surfaces of the sort considered sufficient to give an arbitrary deformation.

Let directions x and z be the principal directions of the Λ-tensor for the plane deformation. The rate of deformation from one set, denoted 'set 1' referred to coordinates x' and z' parallel and normal to it (Fig. 2), is

$$\mathbf{D}_{xx'} = 0 \tag{2a}$$

$$\mathbf{D}_{xz'} = \Delta_1 \mathbf{s}_{xz'} \tag{2b}$$

where Δ_1 is used as a convenient symbol. The two sets will be oriented at angles of ϕ_1 and ϕ_2 to the principal axis x, with one of the angles negative, the angle ϕ_2 say (Fig. 3a). We write $\phi_1 = \phi - \delta$ and $\phi_2 = \phi - \delta$, so the dihedral angle between them is $\phi_1 - \phi_2 = 2\phi$, and set 1 is shifted closer to the x-axis by the bisector of the dihedral angle, δ which should not be confused with the Kronecker delta (δ_{ij}) in equation (1a).

Adding the contributions from the two sets, we obtain,

$$\mathbf{D}_{xx} = \left[\frac{1}{2\eta_n}\right]\mathbf{s}_{xx} \tag{3a}$$

$$\mathbf{D}_{xz} = \left[\frac{1}{2\eta_s}\right]\mathbf{s}_{xz} \tag{3b}$$

where

$$\frac{1}{\eta_n} = (\Delta_1 + \Delta_2)[1 - \cos(4\phi)\cos(4\delta)] - (\Delta_1 - \Delta_2)\sin(4\phi)\sin(4\delta) \tag{3c}$$

$$\frac{1}{\eta_s} = (\Delta_1 + \Delta_2)[1 + \cos(4\phi)\cos(4\delta)] + (\Delta_1 - \Delta_2)\sin(4\phi)\sin(4\delta) \tag{3d}$$

In order that x and z are the principal axes for slip on the two sets of surfaces described above, we require

$$\Delta_1 \sin(4\phi_1) + \Delta_2 \sin(4\phi_2) = 0 \tag{4a}$$

from which we obtain

$$\tan(4\delta) = \left[\frac{(\Delta_1 - \Delta_2)}{(\Delta_1 + \Delta_2)}\right]\tan(4\phi) \tag{4b}$$

Obviously, if $\Delta_1 = \Delta_2$, the principal axis bisects the dihedral angle and $\delta = 0$. If the dihedral angle 2ϕ is small, we may use the linear approximation to equation (4b), obtaining

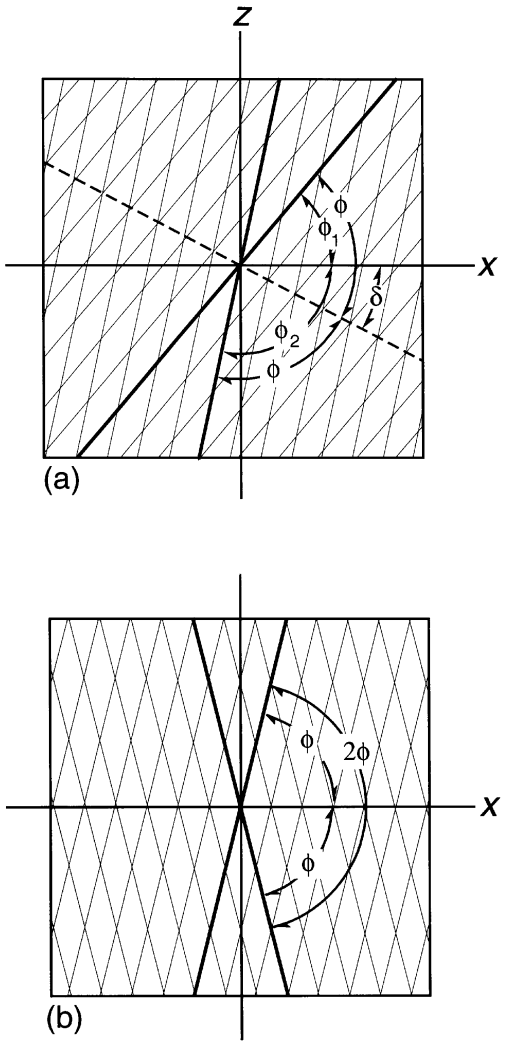

Fig. 3. Intersecting fracture sets (a) with parallel strike, but arbitrary dip (ϕ_1 and ϕ_2). Bisector of the fractures lying closest to the x-axis, has the angle δ with the x-axis, where $-90^\circ \le \delta \le 90^\circ$. Slip along the two fracture sets is allowed to occur simultaneously and without interference. Intersecting fracture sets (b) with parallel strike and equal dip angle, but opposite dip direction. For this case, $\delta = 0$.

$$\delta \cong \left[\frac{(\Delta_1 - \Delta_2)}{(\Delta_1 + \Delta_2)}\right]\phi \tag{5}$$

This shows that for this case, the more compliant, or weaker, set is shifted closer to the x-axis.

The ratio

$$m = \frac{\eta_n}{\eta_s} = \frac{[1 + \cos(4\phi)\cos(4\delta) + \nu \sin(4\phi)\sin(4\delta)]}{[1 - \cos(4\phi)\cos(4\delta) - \nu \sin(4\phi)\sin(4\delta)]} \tag{6a}$$

where

$$\nu = \left[\frac{(\Delta_1 - \Delta_2)}{(\Delta_1 + \Delta_2)}\right] \tag{6b}$$

is a useful measure of the nature of the anisotropy. For $m > 1$, the material is weaker in shear parallel to either of the principal axes than it is in shortening or extension, while for $m < 1$, the opposite holds. For an isotropic material $m = 1$.

Notice that m is not a good measure of the strength or degree of anisotropy, since $m \approx 0$ as well as $m \gg 1$ denote strongly anisotropic materials. An alternate measure of strength of anisotropy is,

$$\mathbf{M} = \left[\frac{\eta_n - \eta_s}{\eta_n + \eta_s}\right] = \left[\frac{m-1}{m+1}\right] \tag{7}$$

which varies from 1 to -1 as m varies from ∞ to 0, and is zero for an isotropic material, $m = 1$.

Notice that the value of m does not change if the value of ϕ is augmented by $\pi/2$. This corresponds to the same configuration of the slip systems, but about the z-axis. As a consequence, we cannot distinguish between the 'instantaneous' bulk behavior of the initial material and one which has four sets of slip surfaces, one pair of which has the same disposition about the z-axis as the pair about the x-axis, except that the viscosities η_n and η_s of the second material will be halved in absolute magnitude.

While the principal axes of a material with a pair of slip systems separated by a dihedral angle, 2ϕ, or a specified value of ν, can be chosen in the above way, one could alternatively choose a pair of principal axes at 45° to the first. To see this, we note that if ϕ_1 and ϕ_2 are solutions to (4a), so are $\phi_1 + (\pi/4)$ and $\phi_2 + (\pi/4)$. The m-value for this choice of principal axes is the reciprocal of the other. That is, if η_n and η_s are the viscosities in x- or z-parallel shortening or extension, and in x- or z-parallel shear, respectively, for the first set of principal axes, then $\eta_n^* = \eta_s$ and $\eta_s^* = \eta_n$ are the corresponding values for the second set of axes.

An example of another anisotropic viscous material may help us to understand this. The material is made up by the repetition of a pair of stiff and soft viscous layers. This material is stiffer in layer-parallel extension or shortening than it is in layer-parallel shear, and, by the first relation, it has the same behavior in layer-normal shortening or extension and layer-normal shear. For the alternate choice of principal axes, at 45° to layering, it is stiffer in shear parallel to one of the principal axes than in shortening or extension.

A thought experiment with this material (which could be readily analyzed in detail) brings out an important point about the present formulation. Consider two experiments, both consisting of the simple shearing of a slab of the layered material. In one, the layering is parallel to the slab surfaces; in the other, it is at right angles to it. A previous comment indicates that, in the first instance, the behavior of both is the same—i.e. the same relationship holds between the rate of shear and the applied shear stress. However, when the layering is parallel to the slab, continued shearing does not effect the behavior, but when the layering is initially normal to the slab, the shearing causes a re-orientation of the layering and a change in the properties, relative to specimen coordinates parallel and normal to the slab. This effect is also present for the materials modeled here, but, in analyzing particular deformations, we do not take it into account. The present formulation approximates the material as one of constant properties. This allows for the rotation of the principal axes of anisotropy in the flow, but it does not allow for the re-orientation of the sets, relative to each other, or for strain-hardening or strain-softening. The approximation should be useful provided the deformation considered is not too large.

In further discussion, we shall simplify matters by supposing that the two sets of surfaces have equivalent slip behaviors, so that $\nu = 0$, and equation (6a) reduces to

$$m = \frac{1 + \cos(4\phi)}{1 - \cos(4\phi)} \tag{8}$$

Figure 4 shows m and $\mathbf{M}$ plotted against 2ϕ.

The form of the relation shown in (8) suggested to one reviewer that the expression for the ratio of principal viscosities was a matter of the geometry of the sets of surfaces alone. The above development indicates that this is not the case.

Notice that for the case of two equivalent sets, $\nu = 0$, when the dihedral angle, 2ϕ, is $\pi/4$, $m = 1$, and the material is isotropic. The corresponding 'fabric' does not look isotropic, but in fact, isotropy or anisotropy refers to a *property* of the material, not the disposition of its internal geometrical elements, and a material may be isotropic with respect to a certain property—for example, thermal conductivity—but not with respect to another—for example, its elastic compliance. The isotropy of this material may be intuitively easier to grasp if it is recalled that its behavior cannot be distinguished from one in which the number of slip systems is doubled, in the manner indicated. The material then possesses four sets of weak surfaces, the angular separation between the two is 45°. If $\nu \neq 0$, the material cannot be isotropic.

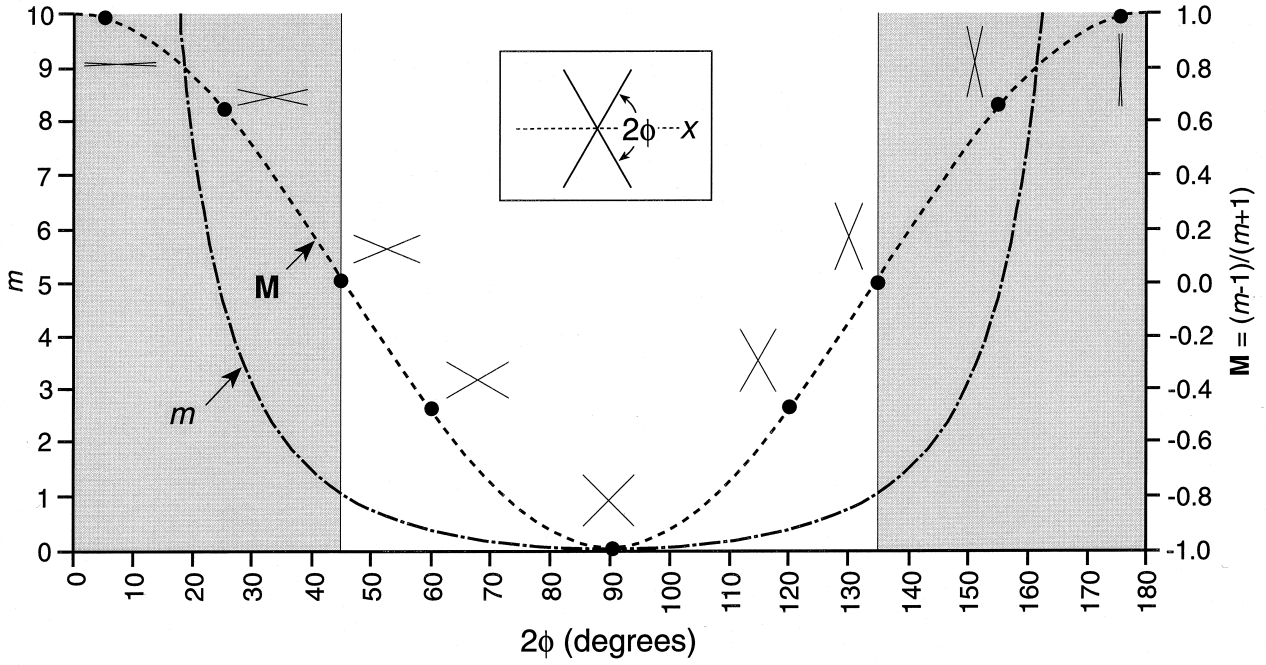

Fig. 4. Plot of anisotropy measures m and $\mathbf{M}$, vs 2ϕ. Schematic fracture orientations (two intersecting lines) located along $\mathbf{M}$ (solid circles) are measured relative to the x-axis (inset).

Modification of the constitutive relations to include matrix deformation

If, in addition to slip on sets of weak surfaces, the intervening elements of sound rock undergo deformation, the relations (3a) and (3b) may be modified. In line with the assumptions already made, let this additional deformation be described by an isotropic, Newtonian viscous law, with viscosity, η_0. We may then write

$$\mathbf{D}_{xx} = \left[\frac{1}{2\eta_{\mathrm{n}}^*}\right]\mathbf{s}_{xx} \tag{9a}$$

$$\mathbf{D}_{xz} = \left[\frac{1}{2\eta_{\mathrm{s}}^*}\right]\mathbf{s}_{xz} \tag{9b}$$

where

$$\frac{1}{\eta_{\mathrm{n}}^*} = \frac{1}{\eta_{\mathrm{n}}} + \frac{1}{\eta_0} \tag{9c}$$

$$\frac{1}{\eta_{\mathrm{s}}^*} = \frac{1}{\eta_{\mathrm{s}}} + \frac{1}{\eta_0} \tag{9d}$$

where η_{n} and η_{s} are the quantities already derived for the slip on the two sets of weak surfaces. Addition of this mechanism decreases the degree of anisotropy. It also allows for arbitrary deformations of the material when there is only a single set of weak surfaces ($2\phi = 0°$), or when the two sets are normal to each other ($2\phi = 90°$).

BOUNDARY VALUE PROBLEMS

To better understand the rheological model, we employ these constitutive relations to examine two frequently modeled structural processes. The first is forced folding (drape folding) of a fractured surface layer due to slip on an underlying, vertical fault. We examine three distinct deformational geometries corresponding to the three behavioral responses discussed above. The second is the buckling, under uniform shortening, of a fractured layer embedded in an isotropic medium. We show plots which display the dominant wavelengths and amplification factors for folds over a given range of bulk viscosity contrasts between the layer and the medium.

Forced-fold models

The deformation of overburden due to slip on a buried vertical fault is a commonly modeled structural configuration (e.g. Sanford, 1959; Reches and Johnson, 1978; Haneberg, 1992, 1993; Patton and Fletcher, 1995). The often cited natural analog for the model consists of a pre-existing vertical fault in crystalline basement overlain by a more compliant, but undeformed, layer of sedimentary rock. The basement blocks to either side of the fault are treated as perfectly rigid, vertically translating past one another as slip occurs along the fault. In practice, the basement blocks themselves are not part of the mathematical

model, but a displacement or velocity field, inferred from their motion, is imparted to the base of the overlying layer (Fig. 5a) as part of the layer's boundary conditions (e.g. Patton and Fletcher, 1995). The upper, planar surface of the layer corresponds to the Earth's surface and is, therefore, stress free (Fig. 5a).

We can envision several geological circumstances which would appropriately alter the homogeneous, isotropic layer(s) assumed in the mathematical studies cited above. An obvious modification is the extreme case where 2ϕ approaches 0° about the x-axis, in which the two near-horizontal surfaces are an analog for a pervasive bedding fabric in the layer. Alternatively, an early deformational event can be envisioned which prepares the rock mass with fractures, which are subsequently reactivated in a later

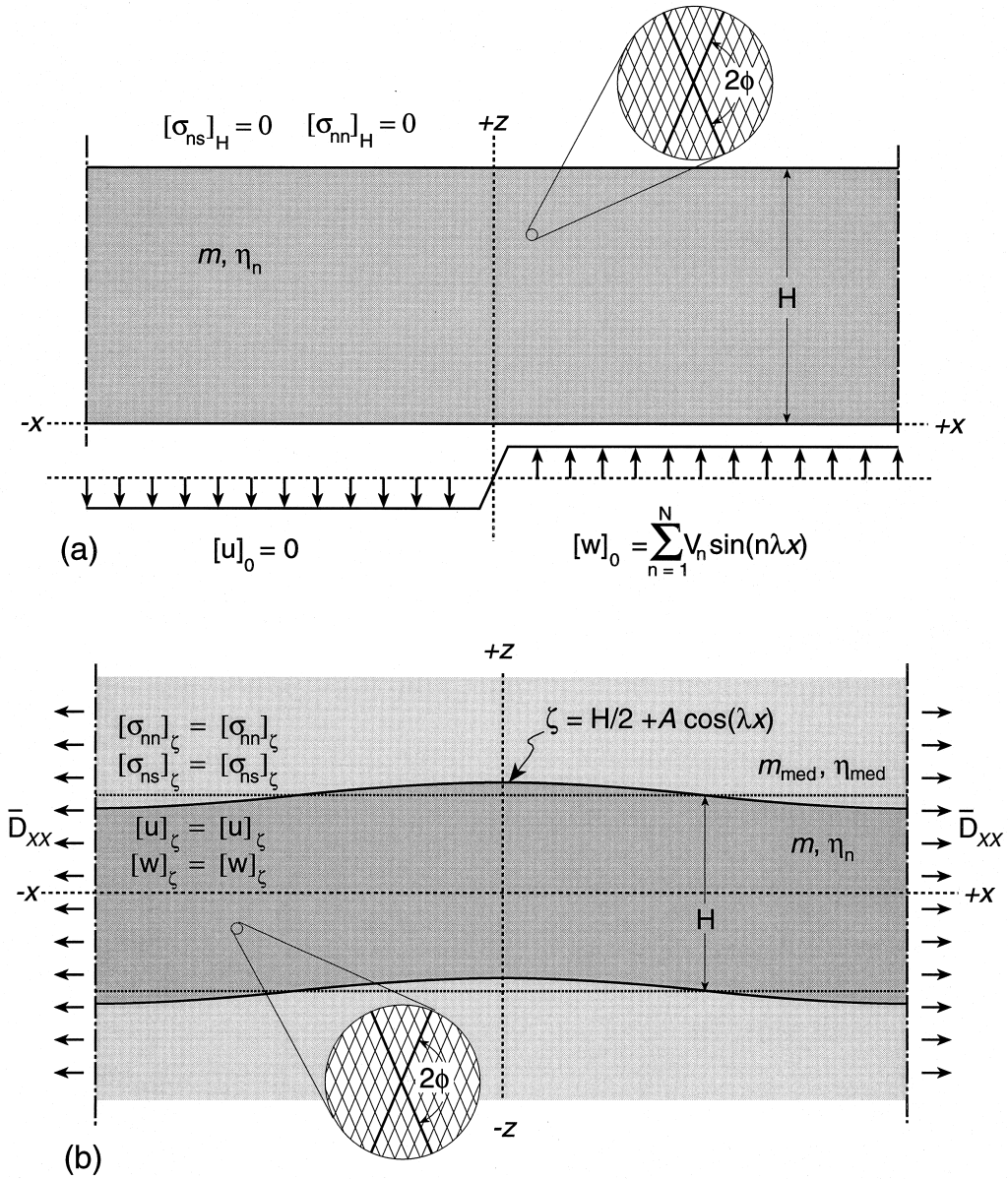

Fig. 5. Mathematical boundary conditions for the two folding models discussed in the text. (a) Forced-fold model for which buried rigid blocks slipping along a vertical planar fault, impart a step-like vertical velocity field to the base of the fractured layer through the truncated series $[w]_0$, the specifics of which are defined in Patton and Fletcher (1995). The horizontal velocity component $[u]$ imparted to the base of the layer is zero. The fractured layer has thickness H and is stress free ($[\sigma_{ns}]_H = [\sigma_{nn}]_H = 0$) at its upper surface. In the layer, m is a function of 2ϕ and η_n is the viscosity of the layer in shortening or extension parallel to the principal axes of anisotropy of the layer. See Patton and Fletcher (1995) for further details on the boundary value problem. (b) Buckling model of a fractured layer with thickness H embedded in an isotropic viscous medium. The model assumes that the sinusoidal interface (ζ) between the medium and the layer is welded, hence shear stresses (σ_{ns}), normal stresses (σ_{nn}), and velocities (u,w) are equal across the interface. The layer is subjected to a layer-parallel deformation rate $\bar{\mathbf{D}}_{xx}$ where a shortening deformation rate is negative. In the medium, $m_{med} = 1$ and η_{med} is its isotropic viscosity. In the layer, m is a function of 2ϕ and η_n is the viscosity of the layer in shortening or extension parallel to the principal axes of anisotropy of the layer. See Johnson and Fletcher (1994) for further details on the boundary value problem.

deformational event. For example, fractured crystalline basement subjected to peneplanation, becomes exposed at the surface. Renewed faulting *at depth* would likely occur along discrete shear zones, since higher confining pressures would homogenize the rock, causing the weak fracture surfaces to be ignored. However, at lower confining pressures near the surface, the same weak surfaces would become active in accommodating the deformation associated with the faults at depth. Alternatively, the deeper fractures could have been healed. In either case, in our conceptual model, the compliant surface layer corresponds to this shallow zone where deformation along the pre-existing surfaces predominates, while the rigid blocks correspond to that portion of the basement dominated by discrete, vertical shear zones.

In order to solve the boundary value problem of interest, we require a stream function (e.g. Patton and Fletcher, 1995). The stream function takes separate forms for the three material behaviors being considered here (i.e. $m > 1$; $m = 1$; $m < 1$). For $m > 1$,

$$\Psi_1 = -\frac{1}{\lambda^2}\left[A_1^{\alpha_1 \lambda z} + A_2^{-\alpha_1 \lambda z} + A_3^{\alpha_2 \lambda z} + A_4^{-\alpha_2 \lambda z}\right]\cos(\lambda x) \tag{10a}$$

where

$$\alpha_1 = \sqrt{2m - 1 + \sqrt{4m^2 - 4m}} \tag{10b}$$

$$\alpha_2 = \sqrt{2m - 1 - \sqrt{4m^2 - 4m}} \tag{10c}$$

For $m = 1$,

$$\Psi_2 = -\frac{1}{\lambda^2}\left\{[B_1 + B_2(\lambda z - 1)]e^{\lambda z} + [B_3 + B_4(\lambda z + 1)]e^{-\lambda z}\right\}\cos(\lambda x) \tag{11}$$

For $m < 1$,

$$\Psi_3 = -\frac{1}{\lambda^2}\left\{[C_1 \cos \beta\lambda z + C_2 \sin \beta\lambda z]e^{\gamma \lambda z} + [C_3 \cos \beta\lambda z + C_4 \sin \beta\lambda z]e^{-\gamma \lambda z}\right\}\cos(\lambda x) \tag{12a}$$

where

$$\beta = \sqrt{1 - m} \tag{12b}$$

$$\gamma = \sqrt{m} \tag{12c}$$

In equations (10)–(12), λ is the wave number $2\pi/L$ and L is the wavelength. From this point forward, solution of the boundary value problem follows treatments presented in Patton and Fletcher (1995).

A small amount of slip on the underlying basement shear zone results in the distortion of the initially square grid elements of the layer (Fig. 6). We have chosen a time increment to yield a fault displacement of 0.12 of the layer thickness. The width of the vertical-fault shear zone at the base of the layer is approximately 0.05 of the fundamental wavelength and approximately 0.4 of the layer thickness. These numerical experiments examine variations in 2ϕ such that m varies through four orders of magnitude.

Figure 6(a) shows the deformation in a layer of rock in which the fractures have either a very small or a very large intersurface angle. We have chosen a value of 10 for m which solving for 2ϕ in equation (8) corresponds to an angle of 17.5° or 162.5°. The most pronounced slip on fractures occurs in a narrow, vertically aligned region within the layer, extending across the entire layer. As a result, the upper surface of the layer displays a velocity profile very similar to that imposed at its base, forming a narrow, steeply dipping monocline (or shear zone) with well defined hinges (or boundaries).

Decreasing the value of m causes the zone of deformation to widen upward forming a wedge-shaped region above the vertical fault in which the deformation becomes more diffuse upwards. Maximum development of the wedge occurs when $m = 1$, the isotropic case (Fig. 6b) for which 2ϕ is equal to 45° or 135°. The profile of the upper surface of the layer forms a wide, gentle monocline with broad hinges.

As we continue to decrease m to values less than unity, deformation becomes localized along the lateral boundaries of the wedge of diffuse deformation developed in the isotropic model. The internal portion of the wedge becomes less and less deformed. At values of $m = 0.1$, corresponding to a 2ϕ of 84.3° or 95.7°, the layer (Fig. 6c) is divided into three relatively undeformed domains separated by two narrow shear-zone-like regions of deformation converging downward to the tip of the underlying vertical fault. The zone towards the up-thrown side of the layer has a normal sense of slip while that towards the down-thrown side displays reverse slip. The upper surface of the layer has taken on a stair-step profile, stepping upwards toward the up-thrown side of the layer. The two shear zones separating the flat regions of the "steps" are expressed at the surface of the layer as two, steep-limbed, narrow monoclines.

Buckling models

As a second example of the effect of anisotropy on deformation, we present results for the two-dimensional, cylindrical folding in plane flow of an anisotropic viscous layer in an isotropic viscous medium, and for the simplest type of internal folding instability in an unbounded volume of the material.

Folding of an anisotropic viscous layer in an isotropic viscous medium. Two types of folding can take place in anisotropic media (Biot, 1965). *Interfacial instability* is

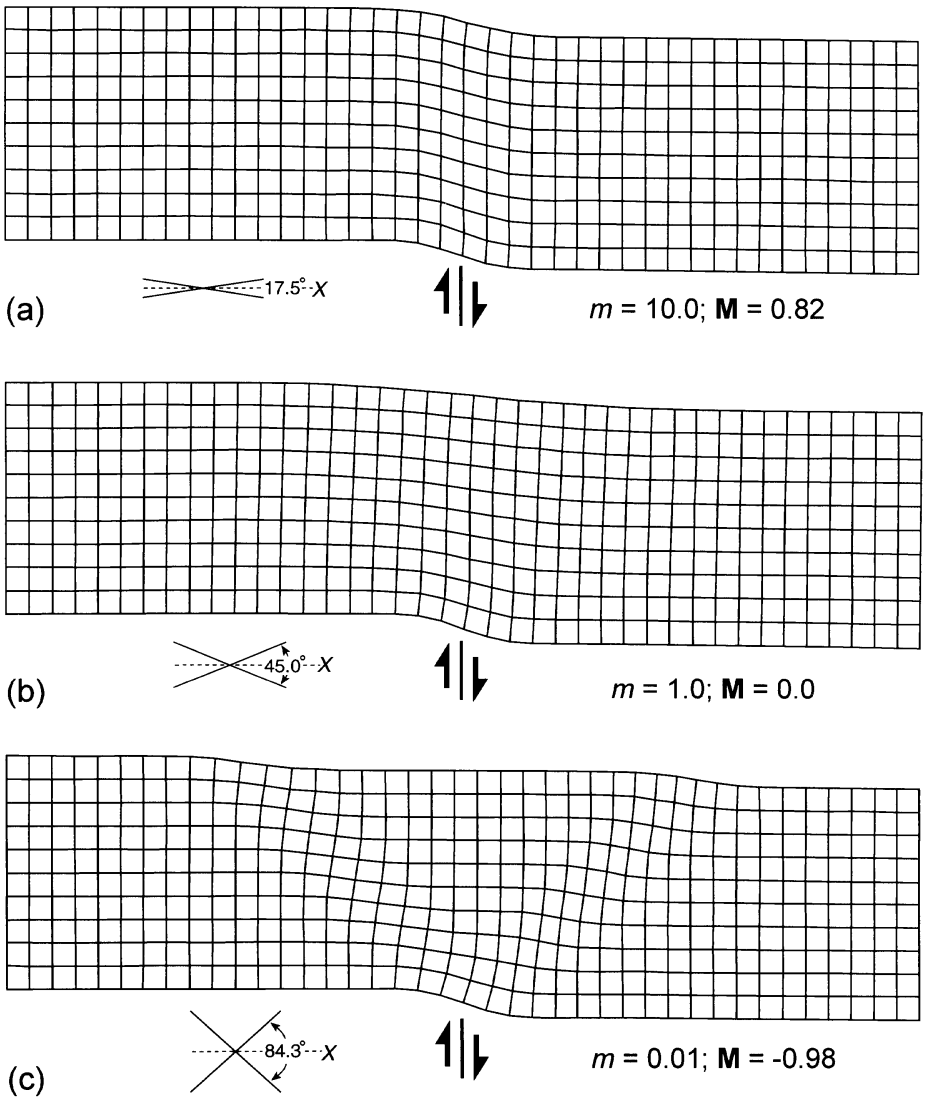

Fig. 6. Deformational response of symmetrically fractured rock layers due to slip on an underlying, vertical basement fault. The intersurface angle 2ϕ is the only parameter varied among the three models, and has values of (a) 17.5° or 162.5°, (b) 45° or 135°, and (c) 84.3° or 95.7°. Schematic diagrams of one of these fracture angles (measured relative to the x axis) and values of m and **M** for each model are shown below the deformed grids.

driven by the jump in the basic-state normal stress difference at an interface between stiff and soft media. *Internal instability* results from amplification of a fluctuation in the orientation of the principal axes of anisotropy within the medium. As an approximation, the two may be treated independently. Here, we first consider the interfacial instability of a stiff anisotropic viscous layer embedded in a soft medium. For simplicity the soft medium is taken to be an isotropic viscous fluid with viscosity η_{med}. In the case considered, the layer-medium interfaces are bonded.

The analysis of low-amplitude folding follows standard lines (Johnson and Fletcher, 1994), and employs the same stream functions (10, 11 and 12) as defined in the forced-fold case. Only the final results are given here. The instantaneous rate of amplification of a fold component with wavelength L and amplitude **A** is given by

$$q|\overline{\mathbf{D}}_{xx}| = \left[\frac{1}{\mathbf{A}}\right]\left[\frac{\mathrm{d}\mathbf{A}}{\mathrm{d}t}\right] \tag{13}$$

where $\overline{\mathbf{D}}_{xx}$ is the uniform deformation rate parallel to the layer boundary (Fig. 5b).

For $m < 1$, the perturbing flow in the anisotropic viscous layer is of the same form as that for an isotropic power-law layer, with stress exponent $n = 1/m$, and

$$q = -\mathrm{Sgn}(\overline{\mathbf{D}}_{xx}) + \frac{2n(1-R)\mathrm{Sgn}(\overline{\mathbf{D}}_{xx})}{(1-Q^2) - \dfrac{(n-1)^{1/2}[(1+Q^2)(\mathrm{e}^{\gamma k}-\mathrm{e}^{-\gamma k})+2Q(\mathrm{e}^{\gamma k}-\mathrm{e}^{-\gamma k})]}{2\sin(\beta k)}} \tag{14}$$

(Fletcher, 1974) where $k = 2\pi[H/L]$, $R = (\eta_{\text{med}}/\eta_{\text{n}})$, H is the layer thickness, and rewriting γ and β (12b and c) in terms of the stress exponent

$$\gamma = \sqrt{\frac{1}{n}}, \quad \beta = \sqrt{1 - \frac{1}{n}} \quad \text{and } Q = \frac{R}{\gamma} \tag{15}$$

Finally, $\text{Sgn}(\overline{\mathbf{D}}_{xx}) = +1$, 0, and -1 for $\overline{\mathbf{D}}_{xx} > 0$, $\overline{\mathbf{D}}_{xx} = 0$, and $\overline{\mathbf{D}}_{xx} < 0$, respectively.

For $m > 1$, it is somewhat less convenient to work out a closed-form solution for q. Instead, it is given by the relations

$$q = -\text{Sgn}(\overline{\mathbf{D}}_{xx}) + A\mathbf{F}_1 + C\mathbf{F}_2 \tag{16a}$$

where

$$\mathbf{F}_1 = \mathrm{e}^{\alpha_1(k/2)} + \mathrm{e}^{-\alpha_1(k/2)} \tag{16b}$$

$$\mathbf{F}_2 = \mathrm{e}^{\alpha_2(k/2)} + \mathrm{e}^{-\alpha_2(k/2)} \tag{16c}$$

where α_2 and α_2 are given in (10b and c) and the quantities A and C satisfy the relations

$$A(\mathbf{G}_1 + \omega\mathbf{F}_1) + C(\mathbf{G}_2 + \omega\mathbf{F}_2) = 0 \tag{16d}$$

$$A(\mathbf{F}_1 + \omega\mathbf{G}_1) + C(\mathbf{F}_2 + \omega\mathbf{G}_2) = \frac{2m}{(2m-1)}(1-R)\text{Sgn}(\overline{\mathbf{D}}_{xx}) \tag{16e}$$

where

$$\omega = \frac{mR}{2m-1} \tag{16f}$$

$$\mathbf{G}_1 = \mathrm{e}^{\alpha_1(k/2)} - \mathrm{e}^{-\alpha_1(k/2)} \tag{16g}$$

$$\mathbf{G}_2 = \mathrm{e}^{\alpha_2(k/2)} - \mathrm{e}^{-\alpha_2(k/2)} \tag{16h}$$

The two quantities which provide a quick assessment of the folding behavior are L_{d}/H, the ratio of the dominant wavelength to the layer thickness (Biot, 1961), and q_{d}, the maximum value of the quantity q—the fold amplification factor—attained at the dominant wavelength. These quantities are plotted in $\mathbf{M}(2\phi)$—$\log_{10}(R)$ space in Fig. 7. Use of $\log_{10}(R)$ provides a convenient spread and form of contours of q_{d} and L_{d}/H; the parameter $\mathbf{M}$ likewise gives a compact and appealing form to the contours. Notice the markedly different dependencies in the two regions, indicated by the change in slope of the contours at the boundary $\mathbf{M} = 0$ ($m = 1$) corresponding to the isotropic layer.

Computation using equation (13) demonstrates that amplification by a factor of 10 in 10% shortening requires $q_{\text{d}} = 23$; at $q_{\text{d}} = 10$, the corresponding amplification is only about three. Hence, a well-developed folding instability is confined to the region in which $q_{\text{d}} > 10$, or, more likely, $q_{\text{d}} \geq 23$. Note that an increase in m leads to a strong decrease in instability in the region $\mathbf{M} > 0$ ($m > 1$). Likewise, in this region, maximum instability occurs at values of L_{d}/H large in comparison to those observed in nature (e.g. Currie *et al.*, 1962). As we shall see shortly, *internal* instability in these materials increases strongly with m, and is the expected form that folding will take.

The region $\mathbf{M} < 0$, or $m < 1$, alternatively describes the initial folding instability for a layer composed of an isotropic, but nonlinear, power-law fluid, or for the presents an anisotropic linear viscous fluid which deforms entirely, or chiefly, by slip on sets of weak surfaces. The strong instability and small L_{d}/H characteristic of the power-law fluid with large stress exponent (Fletcher, 1974; Smith, 1977, 1979) is accordingly also expected in the latter material when the weak surfaces lie close to 45° ($2\phi = 90°$) to the layer surfaces.

Internal instability in an unbounded volume of anisotropic viscous fluid. Here, we consider only the case of shortening parallel to a principal axis of anisotropy. While, in structural geology, internal instability is commonly thought of in terms of the folding of thinly-laminated or foliated material, it can also occur in cases in which the underlying anisotropy arises in other ways.

The simplest mode of instability is one in which the orientation of the principal axis fluctuates sinusoidally in x with angular magnitude $\Theta = \lambda\mathbf{A}$, but with no variation in the z-direction, so that the vertical coordinate of a surface traced so as to be always parallel to the axis, and with mean height, z^*, is

$$\zeta(x, t) = z* + \mathbf{A}\cos(\lambda x) \tag{17}$$

This is the only mode of instability considered here. It is the most unstable mode of instability in shortening parallel to a principal axis chosen so that $\mathbf{M} > 0 (m > 1)$. Analysis of the perturbing flow for (17) yields an expression of the form (13) with

$$q = q_{\text{int}} = -\text{Sgn}(\overline{\mathbf{D}}_{xx})[4(m-1)+1] \tag{18}$$

where q_{int} is the amplification factor for the internal instability. For large m, the instability in shortening, $\text{Sgn}(\bar{\mathbf{D}}_{xx}) = -1$, can be large.

Since, in the plane-flow cases considered here, shortening parallel to one principal axis is equivalent to extension parallel to the other, an instability may also be said to be present in extension. Unlike a layer, the infinite medium has no reference direction, as in the phrase 'layer-parallel shortening'.

Here, however, we shall assume that the considered mode of internal instability is a approximation to that which would occur in a layer of the material embedded in a soft medium. Thus, we may compare q_{int} with the value of q_{d} for the interfacial mode, to roughly assess the relative importance of interfacial instability and internal instability in the folding of the layer. Then, in Fig. 7, the region $m > 1$, or $\mathbf{M} > 0$, is divided into a lower sub-region in which the interfacial mode is dominant in the folding of the layer, and a upper

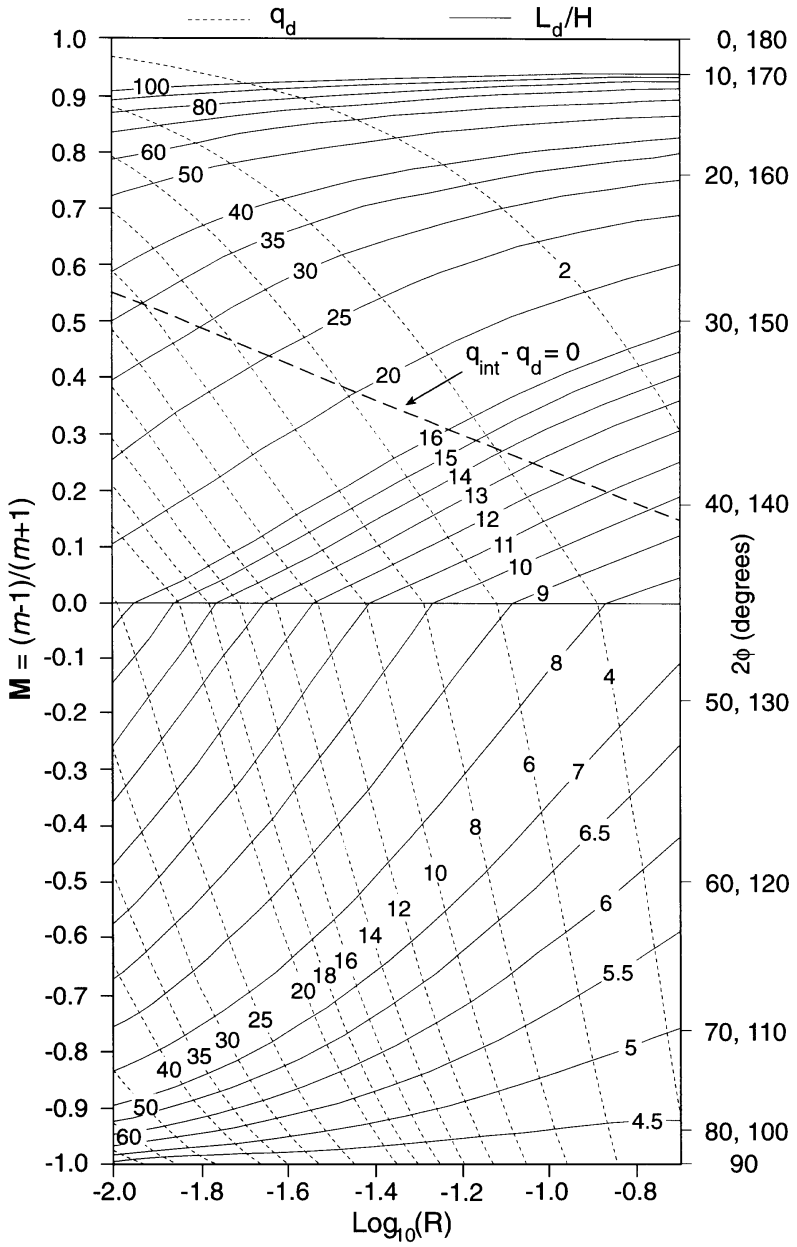

Fig. 7. Contours of L_d/H (the ratio of the dominant wavelength to the layer thickness) and q_d (the maximum value of the quantity q—the fold amplification factor—attained at the dominant wavelength) in $\mathbf{M}(2\phi)$—$\log_{10}(R)$ space.

region in which the internal instability is dominant. The two sub-regions are divided by the locus $q_{int} - q_d = 0$ (Fig. 7).

DISCUSSION

Models describing the deformation of fractured rock can quickly become mathematically unmanageable if we take into account even a few of the geometric, kinematic and dynamic parameters of the process. Nevertheless, simple mathematical models, such as derived here, can provide an appreciation for the deformational responses that might occur in nature.

For the simplified, symmetric two-fracture case considered above, our model predicts that the rock mass will behave as an anisotropic material in all but a very restrictive case. The strength of the anisotropy will have a strongly non linear dependence on the inter-fracture angle, 2ϕ, and may realistically vary by several orders of magnitude. Two extremes in behavior will occur. As $2\phi \rightarrow 0^\circ$ or 180° ($m > 1$, $\mathbf{M} > 0$) the rock mass—when deformed parallel and perpendicular to the principal axes of anisotropy—will be weaker in shear than in shortening or extension. Conversely, when $2\phi \rightarrow 90^\circ$ ($m < 1$, $\mathbf{M} < 0$) the rock mass will be stronger in shear than in shortening or extension. The degree of anisotropy will decrease as $2\phi \rightarrow 45^\circ$ or 135°. When $2\phi = 45^\circ$ or 135° ($m = 1$, $\mathbf{M} = 0$) an iso-

tropic behavior will occur. Although the present treatment emphasizes a symmetric two-fracture system, the model predicts similar types of behaviors for more complex fracture systems as well.

Employing our model in geologically interesting boundary value problems demonstrated a variety of interesting structures. For discussion purposes it is convenient to assume that 2ϕ is measured about the x-axis. Consider first the vertical-fault model in which zones of localized deformation occurred. For the case of a large $2\phi (m > 1, \mathbf{M} > 0)$, the response of the layer (Fig. 6a) was to develop a narrow vertical zone of deformation above the fault. This is an intuitively appealing result in that it is easy to visualize near-vertical fractures ($2\phi \approx 163^\circ$) as an extension of the underlying fault. We might anticipate this response, for example, in an area in which the sedimentary veneer, pervaded by regional fractures, is being deformed by basement-fault reactivation. However, note again that the model makes no mathematical distinction between a fracture array with a large 2ϕ and one with a small, but complimentary angle ($2\phi = 17.5^\circ$). Therefore, we anticipate a similar deformational response for a pervasively bedded section which permits easy slip along near horizontal, weak surfaces (e.g. bedding planes). The resulting deformation geometry in this latter sense would appear geometrically similar to kink bands in foliated rock.

Localized zones of deformation are also predicted for the case where 2ϕ approaches 90° ($m < 1, \mathbf{M} < 0$), in which two 45° dipping planar zones converge downward to the underlying fault (Fig. 6c). Again, this result is intuitively appealing in that we can visualize that the wedge above the fault is exploiting the $\approx 42^\circ$ dipping fractures at its boundary for slip. We might anticipate this type of behavior where a Coulomb material, with a small angle of internal friction, has seen the development of a pervasive set of conjugate fractures, or where orthogonal, intersecting discontinuities (e.g. bedding and fractures) have been rotated to an inclined orientation. The localized zones of deformation described for these two cases ($m > 1$ and $m < 1$) widen and the deformation becomes more diffuse as 2ϕ departs from 0°, 90° and 180° until an isotropic behavior occurs as $2\phi \rightarrow 45^\circ$ or 135° (Fig. 6b).

Our intuition serves us less well when considering the bulk response of a fractured layer to shortening. When we view outcrops pervaded with the products of a brittle process—i.e. fracturing—periodic folds are not what we typically anticipate for the same rock at a larger scale. Yet our mathematical description of one potential behavioral response suggests that such features are possible. Indeed, our model predicts that the angle of the intersection of the fractures controls both the dominant wavelength as well as the rate of amplification of the buckling instability. For a fixed R and H, rocks displaying fractures with $2\phi \approx 90^\circ$ will display strong amplification of short-wavelength folds. As 2ϕ decreases towards the x-axis, longer wavelengths are selected for amplification, but the amplification factor is reduced. For the range of R considered in Fig. 7, when 2ϕ is reduced to a value somewhere between 40° and 30°, the internal instability of the layer grows at a greater rate than the interfacial instability.

The results of these two boundary value problems influence how we might think about natural structures in two ways. First, the mathematical experiments provide deformational geometries which allow for interpretive alternatives when predicting subsurface relationships. For example, the deformation geometries displayed in Fig. 6 are significant departures from those portrayed in mathematical models of isotropic (e.g. Sanford, 1959; Patton and Fletcher, 1995) or layered (e.g. Reches and Johnson, 1978; Stein and Wickham, 1980; Haneberg, 1992, 1993) sequences deformed above vertical faults. Secondly, the deformation geometries of the mathematical experiments emphasize the potential of the fractured mass—despite the relatively brittle behavior of the intervening lithons—to deform in bulk by folding. The results of both of the above mathematical experiments have application to regions in which the brittle vs ductile response of a mechanical unit is at issue, such as the debates concerning the response of the basement in the Wyoming foreland (e.g. Matthews, 1986). Indeed, it is appropriate to consider large-scale symmetric folding—or by analogy to other studies of anisotropic fluids (e.g. Fletcher, 1974; Smith, 1977, 1979), antisymmetric folding—of the crust in light of this model for polyphase deformed basement rocks. For example, the large-scale pinch-and-swell (anti-symmetric folding) mechanism for development of the Basin and Range province proposed by Fletcher and Hallet (1983) could also be attributed to an anisotropy associated with pervasive fractures or faults.

Regardless of the application, rheological models describing the deformation of a fractured rock mass suggest that first-order estimates of their behavior can be made, and that predictable structures will evolve from finite deformations of such masses.

Acknowledgements—We gratefully acknowledge Simon Cox and J. D. St. George for constructive comments on an earlier version of this manuscript.

REFERENCES

Amadei, B. and Goodman, R. E. (1981) Formulation of complete plane strain problems for regularly jointed rocks. *Proceedings of the 22nd U.S. Symposium on Rock Mechanics, Rock Mechanics From Research to Application*. (Compiled by H. H. Einstein) Massachusetts Institute of Technology, pp. 245–251.

Biot, M. A. (1961) Theory of folding of stratified viscoelastic media and its implications in tectonics and orogenesis. *Geological Society of America Bulletin* **72,** 1595–1620.

Biot, M. A. (1965) *Mechanics of Incremental Deformations*. John Wiley, New York.

Currie, J. B., Patnode, H. W. and Trump, R. P. (1962) Development of folds in sedimentary strata. *Geological Society of America Bulletin* **73,** 655–674.

Fletcher, R. C. (1974) Wavelength selection in the folding of a single layer with power-law rheology. *American Journal of Science* **274,** 1029–1043.

Fletcher, R. C. and Hallet, B. (1983) Unstable extension of the lithosphere: A mechanical model for Basin-and-Range structure. *Journal of Geophysical Research* **88,** 7457–7466.

Haneberg, W. C. (1992) Drape folding of compressible elastic layers—I. Analytical solutions for vertical uplift. *Journal of Structural Geology* **14,** 713–721.

Haneberg, W. C. (1993) Drape folding of compressible elastic layers—II. Matrix solution for two-layer folds. *Journal of Structural Geology* **15,** 923–932.

Johnson, A. M. and Fletcher, R. C. (1994) *Folding of Viscous Layers*. Columbia University Press, New York.

Matthews, V. III (1986) A case for brittle deformation of the basement during the Laramide Revolution in the Rocky Mountain Foreland Province. *The Mountain Geologist* **23,** 1–5.

Morland, L. W. (1976) Elastic anisotropy of regularly jointed media. *Rock Mechanics* **8,** 35–48.

Patton, T. L. and Fletcher, R. C. (1983) Simple rheological model for rock with multiple fracture sets: application to the deformation of a fractured surface layer above a deep basement fault. 1983, 96th Annual Meeting. *Geological Society of America* **15,** Abstracts with programs 659.

Patton, T. L. and Fletcher, R. C. (1995) Mathematical block-motion model for deformation of a layer above a buried fault of arbitrary dip and sense of slip. *Journal of Structural Geology* **17,** 1455–1472.

Reches, Z. (1978) Development of monoclines: Part I. Structure of the Palisades Creek branch of the Eastern Kaibab monocline, Grand Canyon, Arizona. In *Laramide Folding Associated with Basement Block Faulting in the Western United States*, ed. V. Matthews, III. pp. 235–271, Geological Society of America Memoir, **151**.

Reches, Z. (1979) Deformation of a foliated medium. *Tectonophysics* **57,** 119–129.

Reches, Z. and Johnson, A. M. (1978) Development of monoclines: Part II. Theoretical analysis of monoclines. In *Laramide Folding Associated with Basement Block Faulting in the Western United States*, ed. V. Matthews, III. pp. 273–311, Geological Society of America Memoir, **151**.

Robin, P-Y. and Currie, J. B. (1971) Analysis of fracturing in the Precambrian volcanics north of Madoc, Ontario. *Canadian Journal of Earth Sciences* **8,** 1302–1313.

Sanford, A. R. (1959) Analytical and experimental study of simple geologic structures. *Geological Society of America Bulletin* **70,** 19–52.

Segall, P. and Pollard, D. D. (1983a) Nucleation and growth of strike slip faults in granite. *Journal of Geophysical Research* **88,** 555–568.

Segall, P. and Pollard, D. D. (1983b) Joint formation in granitic rock in the Sierra Nevada. *Geological Society of America Bulletin* **94,** 563–575.

Smith, R. B. (1977) Formation of folds, boudinage, and mullions in non-Newtonian materials. *Geological Society of America Bulletin* **88,** 312–320.

Smith, R. B. (1979) The folding of a strongly non-Newtonian layer. *American Journal of Science* **279,** 272–287.

Stein, R. and Wickham, J. (1980) Viscosity-based numerical model for fault-zone development in drape folding. *Tectonophysics* **66,** 225–251.

Walcott, C. D. (1890) Study of line displacement in the Grand Canyon of the Colorado in northern Arizona. *Geological Society of America Bulletin* **1,** 49–64.